

Quantum Criticality of Liquid-Gas Transition in a Binary Bose Mixture

Li He,^{1,*} Haowei Li,^{2,*} Wei Yi,^{2,3} and Zeng-Qiang Yu^{4,5,†}

¹College of Physics and Electronic Engineering, Shanxi University, Taiyuan 030006, China

²CAS Key Laboratory of Quantum Information, University of Science and Technology of China, Hefei 230026, China

³CAS Center For Excellence in Quantum Information and Quantum Physics, Hefei 230026, China

⁴Institute of Theoretical Physics, Shanxi University, Taiyuan 030006, China

⁵State Key Laboratory of Quantum Optics and Quantum Optics Devices, Shanxi University, Taiyuan 030006, China

Quantum liquid, in the form of self-bound droplet, is stabilized by a subtle balance between the mean-field contribution and quantum fluctuations. While a liquid-gas transition is expected when such a balance is broken, it remains elusive whether liquid-gas critical points exist in the quantum regime. Here we study the quantum criticality in a binary Bose mixture undergoing the liquid-gas transition. We show that, beyond a narrow stability window of the self-bound liquid, a liquid-gas coexistence persists, which eventually transits into a homogeneous mixture. Importantly, we identify two distinct critical points where the liquid-gas coexistence terminates. These critical points are characterized by rich critical behaviors in their vicinity, including divergent susceptibility, unique phonon-mode softening, and enhanced density correlations. The liquid-gas transition and the critical points can be readily explored in ultracold atoms confined to a box potential. Our work unveils the intriguing quantum liquid-gas criticality, and paves the way for further studies of the rich many-body phenomena in quantum liquids.

Introduction. Liquid-gas transition is ubiquitous in nature, and serves as a paradigm of classical phase transitions. A well-known feature therein is the presence of critical points that mark the onset (or termination) of the liquid-gas coexistence [1]. In the quantum regime, exotic self-bound liquid states (dubbed quantum droplets) have recently been discovered in dipolar or binary Bose-Einstein condensates [2–12], and experimental observations consistent with the liquid-gas coexistence have been reported in imbalanced mixtures [9–12]. The discovery has stimulated extensive interest [13–52], culminating in the latest observation of dipolar supersolids in droplet crystals [53–58]. However, little is known about the transition between the inhomogeneous liquid-gas coexistence and the homogeneous liquid or gas phases. A further important question is whether there exists a quantum analog of the critical point in experimentally relevant systems. Since quantum fluctuations play a key role in the formation of self-bound droplets [2, 15–18], they could lead to yet unexplored many-body phenomena at the critical points. A systematic investigation of such quantum criticality would therefore offer further insight into quantum liquids and enrich our understanding of quantum phase transitions in general.

In this work, we address the questions above by studying the liquid-gas transition in a three dimensional binary Bose mixture with varying densities of its components. We find that, besides the self-bound state which is stable within a narrow window of densities [2], two types of liquid-gas mixtures generally exist, each with a distinct and fully polarized gas component (see Fig. 1). Upon further tuning the densities, the system undergoes a transition from a liquid-gas coexisting state to a homogeneous phase. Starting from the equation of state (EOS) with beyond-mean-field corrections, we quantita-

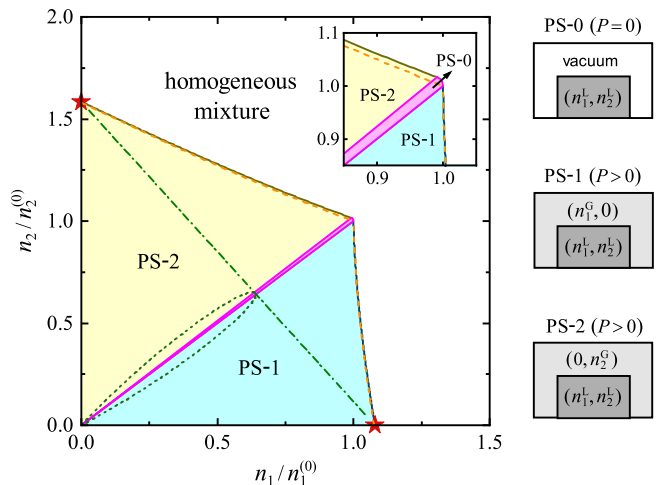


FIG. 1: Left: Ground-state phase diagram of a binary Bose mixture in the mean-field-unstable regime. The phase-separated states PS-1 and PS-2 terminate at the critical points denoted by \star . Dashed lines: phase boundaries given by Eq. (7) and its counterpart with an exchange of species index. The dash-dotted (dotted) line is the diffusive (mechanical) spinodal. Inset: enlarged view in the vicinity of $(n_1^{(0)}, n_2^{(0)})$. Right: illustrations of various inhomogeneous states with either zero or positive pressure. For all figures throughout this work, $\delta\tilde{g} = -0.08$, and $\lambda = 0.68$, which are relevant for spin mixtures of ^{39}K atoms [8–10].

tively characterize the phase diagram, and, crucially, reveal two critical points where the liquid-gas coexistence terminates. Driven by density fluctuations, rich critical phenomena arise near the critical points, exemplified by the divergent susceptibility, the phonon-mode softening, and a dramatic enhancement of the correlation length. Given the recent progress in trapping and probing cold atoms, both the transition and quantum criticality re-

ported here can be readily investigated in a box potential [59].

Liquid-Gas Coexistence. We consider a three dimensional Bose mixture of cold atoms confined in a box of volume V at zero temperature. The system features short-range interactions, with the interaction strengths g_{ij} ($i, j = 1, 2$ labeling the atomic species). Here we consider interspecies attraction and intraspecies repulsion, with $g_{12} < 0$ and $g_{11}, g_{22} > 0$. On the mean-field level, the system would collapse when $g_{12} < -g$, with $g \equiv \sqrt{g_{11}g_{22}}$. Such instability, however, can be dramatically modified once the quantum fluctuations are taken into account [2]. We focus on the regime where $\delta\tilde{g} \equiv 1 + g_{12}/g$ is very small. It follows that, for a homonuclear mixture with equal masses ($m_1 = m_2 = m$), the energy per volume can be written as [2]

$$\mathcal{E} = \sum_{i,j=1,2} \frac{g_{ij}}{2} n_i n_j + \frac{8m^{3/2}}{15\pi^2 \hbar^3} (g_{11}n_1 + g_{22}n_2)^{5/2}, \quad (1)$$

where n_1 and n_2 are the densities of the two species, respectively, \hbar is the reduced Planck constant, and the second term is the Lee-Huang-Yang corrections [60].

The EOS (1) is based on the presumption that the ground state is homogeneous. Yet, this is not true in the low-density limit under the mean-field instability. For a concentration n_1/n_2 fixed at $\lambda \equiv \sqrt{\frac{g_{22}}{g_{11}}}$, the attractive and the repulsive mean-field contributions are mostly cancelled out, and the energy per particle reaches its minimum at the density [2]

$$n_i^{(0)} = \frac{25\pi}{1024 a^3} \sqrt{\frac{g}{g_{ii}}} \frac{\lambda^{5/2}}{(1+\lambda)^5} \delta\tilde{g}^2, \quad (2)$$

with $a \equiv \sqrt{a_{11}a_{22}}$ ($a_{ij} = \frac{mg_{ij}}{4\pi\hbar^2}$ the s -wave scattering length). As a result, when the total atom density fulfills $n < n^{(0)}$, a self-bound liquid state is formed. Here $n^{(0)} = n_1^{(0)} + n_2^{(0)}$. Such a state, referred to as PS-0 in Fig. 1, is stable even if the container of the system is removed, typical of the quantum droplet [8, 9].

The realization of the quantum droplet is not restricted to the exact density ratio λ . Thermodynamically, a stable self-bound liquid can be achieved under the conditions [23, 41]

$$P(n_1, n_2) = 0, \quad \mu_1(n_1, n_2) \leq 0, \quad \mu_2(n_1, n_2) \leq 0, \quad (3)$$

where P is the pressure, and μ_i is the chemical potential of species i . These conditions can be fulfilled within a narrow window of concentration, where the density of the self-bound liquid remains unchanged up to terms of the order $\delta\tilde{g}^2$ [2].

If the population of species 1 increases further, such that the inequality $\mu_1 \leq 0$ no longer holds, the PS-0 state will evolve into an inhomogeneous state with liquid-gas

coexistence (PS-1 in Fig. 1). The balance conditions for the phase separation are given by

$$P(n_1^L, n_2^L) = P(n_1^G, 0), \quad (4)$$

$$\mu_1(n_1^L, n_2^L) = \mu_1(n_1^G, 0), \quad (5)$$

$$\mu_2(n_1^L, n_2^L) < \mu_2(n_1^G, 0), \quad (6)$$

where n_1^L and n_2^L denote the densities of different species in the mixed liquid, and n_1^G is the density of the coexisting gas of species 1. Such liquid-gas coexistence has been studied numerically [33, 50, 52], but the phase transition between the phase-separated state and a homogeneous one is not yet well-understood.

Indeed, the PS-1 state appears only at sufficiently low densities. Its boundary with the homogeneous phase can be derived from Eqs. (4) and (5) by eliminating the variable n_1^G . Keeping densities to the leading order in $\delta\tilde{g}^2$, we analytically derive the phase boundary in a dimensionless form [61]

$$3(1+\lambda)^{5/2} (\tilde{n}_2^L)^2 - (\tilde{n}_1^L + \lambda\tilde{n}_2^L)^{3/2} [(5+3\lambda)\tilde{n}_2^L - 2\tilde{n}_1^L] - 2(\tilde{n}_1^L - \tilde{n}_2^L)^{5/2} = 0, \quad (7)$$

where $\tilde{n}_i^L = n_i^L/n_i^{(0)}$. As shown in Fig. 1, the prediction of (7) is in good agreement with numerical calculations for small $\delta\tilde{g}$.

By tuning the density ratio, one can also realize another kind of liquid-gas coexistence, the PS-2 state, where the gas phase only consists of atoms of species 2. Its phase boundary can be readily obtained by enforcing $\tilde{n}_1^L \leftrightarrow \tilde{n}_2^L$ and $\lambda \rightarrow \lambda^{-1}$ in Eq. (7).

To shed more light on the phase-separated states, we introduce n_+ and n_- to discern what we call the hard and soft degrees of freedom in response to the density variation [2]

$$\begin{pmatrix} n_+ \\ n_- \end{pmatrix} = \begin{pmatrix} \cos\theta & -\sin\theta \\ \sin\theta & \cos\theta \end{pmatrix} \begin{pmatrix} n_1 \\ n_2 \end{pmatrix}, \quad (8)$$

with $\theta = \arctan \lambda$. A geometric interpretation of Eq. (8) can be clearly seen from the inset of Fig. 2. For a given n_+ , the allowed values of n_- must be greater than the physical bound n_-^{\min} , where the system becomes a single-species gas. In the low-density regime, since $\left| \frac{\partial\mu_i}{\partial n_+} \right| \gg \left| \frac{\partial\mu_i}{\partial n_-} \right|$, the thermodynamic balance requires the hard-mode variable n_+ to be almost invariant in the coexisting phase (hence the name hard mode), enabling a single-mode approximation. As shown in Fig. 2, when n_+ lies within an appropriate range (expression given later), $\mathcal{E}(n_-)$ changes from concave to convex in the starting segment, meaning the energy of the phase-separated state (dashed lines) is lower than that of the homogenous state. The coexistence condition is thus

$$(n_-^L - n_-^{\min}) \left. \frac{\partial\mathcal{E}}{\partial n_-} \right|_{n_-^L} = \mathcal{E}(n_+, n_-^L) - \mathcal{E}(n_+, n_-^{\min}). \quad (9)$$

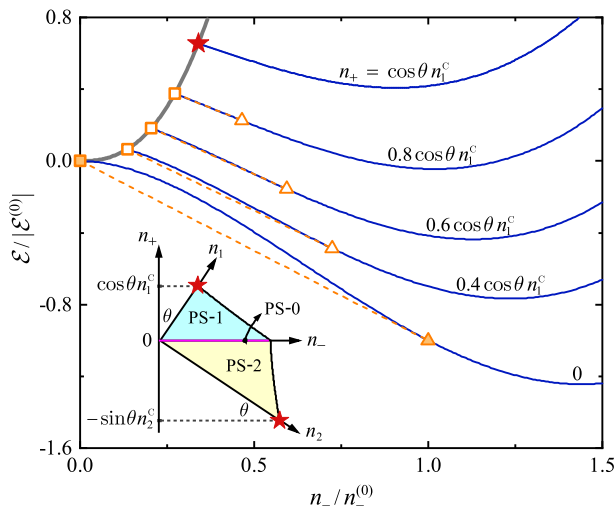


FIG. 2: EOS with the density variable n_+ fixed at different values. The dashed segments correspond to the energy of the inhomogeneous states. \square and \triangle denote the coexisting liquid and gas phase, respectively. The filled symbols highlight the case of $n_+ = 0$, where the liquid is self-bound. The gray bold line represents the EOS of a pure gas of species 1. For a better view, \mathcal{E} is shifted by $\frac{1}{2}(g_{11} + g_{22})n_+^2$. $\mathcal{E}^{(0)} = \frac{1}{3}(g + g_{12})n_1^{(0)}n_2^{(0)}$ is energy density of the self-bound state. The density variable n_- is measured in the unit of $n_-^{(0)} \equiv n_1^{(0)} \sin \theta + n_2^{(0)} \cos \theta$. Inset: phase diagram obtained in the single-mode approximation. \star denotes the critical points.

For positive n_+ , Eq. (9) reproduces the result obtained in (7); for negative n_+ , it gives the boundary of the PS-2 state [61].

We note that the phase boundary predicted by the single-mode approximation is accurate only to the leading order in $\delta\tilde{g}^2$. At this level the stable region of the PS-0 state collapses onto the n_- axis (see inset of Fig. 2). Further, when $\delta\tilde{g}$ becomes large, terms neglected in the Lee-Huang-Yang contribution in Eq. (1) would result in a higher-order shift of the phase boundary.

Quantum Criticality. In part of the coexistence region, the homogeneous phase appears as a metastable state, similar to the superheated liquid in the classical liquid-gas transition [1]. Across the diffusive spinodal line fixed by $\gamma_1\gamma_2 = \gamma_{12}^2$ ($\gamma_i \equiv \frac{\partial\mu_i}{\partial n_i}$ and $\gamma_{12} \equiv \frac{\partial\mu_1}{\partial n_2}$), a homogeneous state becomes dynamically unstable. Note that the mechanical spinodal line, along which the compressibility diverges, lies inside the unstable region (see Fig. 1).

According to Eq. (1), the diffusive spinodal line can be explicitly written as $n_1/n_1^c + n_2/n_2^c = 1$, and it meets the phase boundaries of PS-1 and PS-2 at the critical points $(n_1^c, 0)$ and $(0, n_2^c)$, respectively. To the leading order in $\delta\tilde{g}^2$, we find a simple expression for these critical points

$$n_i^c = \frac{16}{25} \left(1 + \frac{g}{g_{ii}} \right) n_i^{(0)}, \quad (10)$$

where the liquid-gas transitions terminate. In the representation of (n_+, n_-) , the liquid-gas coexistence only occurs within the interval $-\sin\theta n_2^c < n_+ < \cos\theta n_1^c$, while the homogeneous ground state evolves smoothly at either larger or smaller n_+ , reminiscent of the supercritical regime of a classical liquid-gas transition.

Importantly, in the vicinity of these critical points, density fluctuations dominate and give rise to rich critical behaviors. Such quantum criticality is manifested in the singular behavior of the static susceptibilities χ_{ij}^0 (i, j label the atom species) in response to density perturbations, with

$$\chi_{ii}^0 = \frac{\gamma_{3-i}}{\gamma_1\gamma_2 - \gamma_{12}^2}, \quad \chi_{12}^0 = \chi_{21}^0 = \frac{-\gamma_{12}}{\gamma_1\gamma_2 - \gamma_{12}^2}. \quad (11)$$

Here the susceptibilities are constructed from the species-resolved response functions following a hydrodynamic approach [61]. Since the coexistence boundaries meet the spinodal line at the critical points, all χ_{ij}^0 become divergent there.

Another related critical phenomenon is the softening of the phonon excitations. Specifically, the sound velocities of the phonon modes are [61]

$$c_{\pm} = \sqrt{\frac{1}{2m} \left[\gamma_1 n_1 + \gamma_2 n_2 \pm \sqrt{(\gamma_1 n_1 - \gamma_2 n_2)^2 + 4\gamma_{12}^2 n_1 n_2} \right]}, \quad (12)$$

where c_- vanishes at either critical point. At the first glance, this seems quite natural, since only one phonon mode can survive as the density of the minority species approaches zero. However, it is only at the critical points that c_- exhibits a unique linear dependence on the vanishing minority density. For instance, in the low-concentration limit with $n_1 = n_1^c$, the sound velocity $c_- = \frac{5\sqrt{\Delta}}{2\sqrt{2}} c_-^{(0)} \tilde{n}_2$, where $\tilde{n}_2 = n_2/n_2^{(0)}$, and $c_-^{(0)} = 4\sqrt{gn^{(0)}\sqrt{n^{(0)}a^3}/5\sqrt{\pi}m}$ is the sound velocity of the self-bound liquid [61]. In contrast, we find $c_- \propto \sqrt{\tilde{n}_2}$ in the low-concentration limit with a fixed $n_1 > n_1^c$. Such distinction (see Fig. 3(a)) provides a clear signature for detecting the critical points.

The quantum criticality is also manifested in the dramatic changes in the correlation length. The relative probability of finding two particles of a given species at distance r is measured by the pair-distribution function $\mathcal{D}_{ij}(r) \equiv \frac{1}{n_i n_j} \langle \hat{\Psi}_i^\dagger(\mathbf{r}) \hat{\Psi}_j^\dagger(\mathbf{0}) \hat{\Psi}_j(\mathbf{0}) \hat{\Psi}_i(\mathbf{r}) \rangle$, with $\hat{\Psi}_i(\mathbf{r})$ the field operator and $r = |\mathbf{r}|$. At large distances, the asymptotic form of \mathcal{D}_{ij} reads [66, 67]: $\mathcal{D}_{ij}(r \rightarrow \infty) = 1 - \frac{\xi_{ij}}{\sqrt{2n_i n_j \pi^2 r^4}}$, where ξ_{ij} is the correlation length [66]. Thus, the combined length scale $(\xi_{ij}/\sqrt{n_i n_j})^{1/4}$ represents a characteristic distance, over which \mathcal{D}_{ij} deviates considerably from unity.

At a critical point, for instance $n_1 = n_1^c$ and $n_2 \rightarrow 0$,

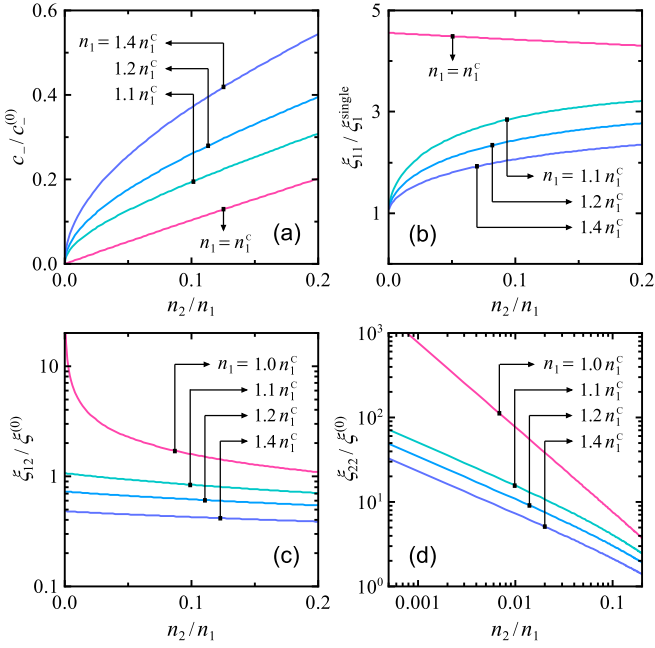


FIG. 3: Sound velocity c_- and correlation lengths ξ_{ij} as functions of the minority concentration n_2/n_1 , for different n_1 .

ξ_{ij} behaves like [61]

$$\xi_{11} \rightarrow \xi_1^{\text{single}} \left(1 + \frac{1}{\sqrt{|\delta\tilde{g}|}} \right), \quad (13)$$

$$\xi_{12} \sim \frac{\xi^{(0)}}{\sqrt{\tilde{n}_2}} \rightarrow \infty, \quad \xi_{22} \sim \frac{\xi^{(0)}}{\tilde{n}_2} \rightarrow \infty, \quad (14)$$

where $\xi_1^{\text{single}} = \hbar/\sqrt{2mn_1\gamma_1}|_{n_2=0}$ is the healing length of a single-species Bose gas [66, 68], $\xi^{(0)} = \frac{\sqrt{3\hbar(\sqrt{g_{11}}+\sqrt{g_{22}})}}{g\sqrt{2m|\delta\tilde{g}|n^{(0)}}}$ is the typical surface thickness of a self-bound droplet [2]. By contrast, for the case with any given $n_1 > n_1^c$ (and $n_2 \rightarrow 0$), we have [61]

$$\xi_{11} \rightarrow \xi_1^{\text{single}}, \quad \xi_{12} \rightarrow A\xi^{(0)}, \quad \xi_{22} \sim \frac{\xi^{(0)}}{\sqrt{\tilde{n}_2}} \rightarrow \infty, \quad (15)$$

where the coefficient A is defined in the Supplemental Material. The distinction between these two situations, as illustrated in Fig. 3(a)-(c), reflects the significant enhancement of density correlations at the quantum criticality, and can be tested experimentally using the Bragg spectroscopy. Note that the discussions above apply to the other critical point by exchanging the species labels.

It is worth noting that the structures of the PS-1 and PS-2 states resemble that of the partially miscible states recently predicted for $g_{12} > g$ [69], where the Lee-Huang-Yang correction also plays a crucial role in establishing the coexistence equilibrium. The key difference is that, under the repulsive interspecies interactions in Ref. [69], the spinodal instability is due to the out-of-phase fluctuations of the two species; while in our case ($g_{12} < -g$),

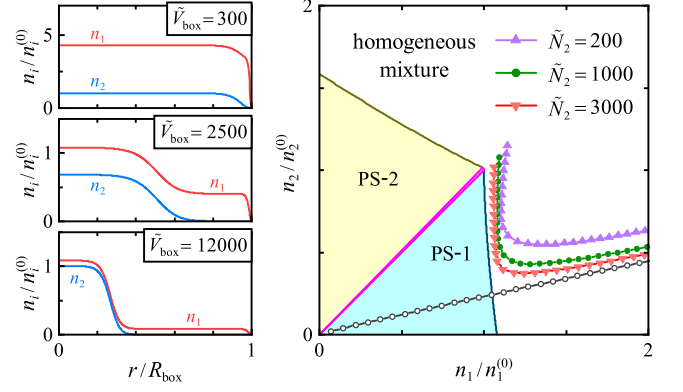


FIG. 4: Left: Atomic density profiles in a box trap of different sizes with $(\tilde{N}_1, \tilde{N}_2) = (5000, 1000)$. Right: Trajectory of the central density during an adiabatic expansion with various atom numbers. For comparison, the result for the case with $\delta\tilde{g} = 0$ and $\tilde{N}_2 = 3000$ is also shown (o). All the simulations are performed with the concentration $\tilde{N}_1/\tilde{N}_2 = 5$.

the quantum criticality originates from the in-phase fluctuations.

Density Profiles. The predicted phase diagram can be experimentally verified with ultracold atoms confined in a box potential [59]. We numerically simulate the atomic density profiles by solving the extended Gross-Pitaevskii equation [2]

$$\left[-\frac{\hbar^2\nabla^2}{2m} + \frac{\partial}{\partial n_i} \mathcal{E}(n_1(\mathbf{r}), n_2(\mathbf{r})) - \bar{\mu}_i^{\text{box}} \right] \psi_i(\mathbf{r}) = 0, \quad (16)$$

where ψ_i is the condensate wavefunction satisfying $\psi_i = 0$ at the boundary of the box, and $\bar{\mu}_i^{\text{box}}$ is the global chemical potential fixed by the normalization condition $\int d\mathbf{r} |\psi_i(\mathbf{r})|^2 = N_i$. For simplicity, we consider a spherical box trap of radius R_{box} , and introduce dimensionless variables $\tilde{N}_i = N_i/n_i^{(0)}\xi^{(0)3}$ and $\tilde{V}_{\text{box}} = (R_{\text{box}}/\xi^{(0)})^3$.

As illustrated in the left column of Fig. 4, for sufficiently small \tilde{V}_{box} , the atomic densities are almost uniform, except for a thin layer close to the boundary. When \tilde{V}_{box} increases beyond a certain threshold, the liquid-gas coexistence appears, and the density profile exhibits a shell structure, with a liquid core immersed in a single-component gas of the majority species. Here the densities of the two coexisting phases roughly obey the relation $\tilde{n}_1^c = \tilde{n}_1^l - \tilde{n}_2^l$ with $\tilde{n}_i^c = n_i^c/n_i^{(0)}$, consistent with results from the single-mode approximation. As \tilde{V}_{box} further increases, the gas in the outer shell becomes extremely dilute, and the liquid core is essentially self-bound with the densities approaching the saturated values $(n_1^{(0)}, n_2^{(0)})$. These results imply that, under the liquid-gas coexistence, a clear distinction between the gas phase and the liquid phase can be observed during an adiabatic expansion—while the outer gas shell diffuses throughout the box, the liquid core retains a finite volume.

Further, the phase diagram can be readily extracted

from the flattop density profile. The right panel of Fig. 4 shows the evolution of the central density when \tilde{V}_{box} gradually increases at a fixed concentration $\tilde{N}_1/\tilde{N}_2 = 5$. As the phase separation sets in, the density trajectory turns upward abruptly and follows the phase boundary of the PS-1 state. Such a behavior is in stark contrast to the case without the liquid-gas transition (empty circles). By choosing a concentration $\tilde{N}_1/\tilde{N}_2 \ll 1$, the boundary of PS-2 state can also be obtained.

Due to the finite-size effect, the phase boundary constructed in this way shows some deviations from that in the thermodynamic limit. The deviation becomes less pronounced when $\tilde{N}_i \gtrsim 1000$ (see Fig. 4). Under our choice of parameters (see Fig. 1), the condition $(\tilde{N}_1, \tilde{N}_2) = (1, 1)$ corresponds to $(N_1, N_2) = (1.16, 1.71) \times 10^3$, which means that experiments with atom numbers of the order 10^6 should suffice.

Discussion. In summary, we have shown that, a mean-field unstable binary Bose mixture hosts two kinds of liquid-gas coexistence, each terminating at a distinct critical points. Rich critical phenomena arise at these points, which are detectable in current cold-atom experiments. The liquid-gas transition considered here also occurs in heteronuclear mixtures such as ^{41}K - ^{87}Rb [11] and ^{23}Na - ^{87}Rb [12]. Therein, the beyond-mean-field correction cannot be written in an analytic form [2], and the determination of the phase boundaries is thus more involved. Nevertheless, for $|\delta\tilde{g}| \ll 1$, the Lee-Huang-Yang energy can be approximated as [31, 49]: $\mathcal{E}_{\text{LHY}} = \frac{8}{15\pi^2\hbar^3} \left(m_1^{3/5} g_{11} n_1 + m_2^{3/5} g_{22} n_2 \right)^{5/2}$. The results of this work would then still hold, with the replacement $\lambda \rightarrow \lambda \left(\frac{m_2}{m_1} \right)^{3/5}$ in Eqs. (2), (7) and (10) [61].

For future studies, it is desirable to generalize our results to lower dimensions [14, 25, 26, 30, 35, 42], with three-body interactions [70, 71], or to finite temperatures [39, 40, 46–48]. At finite temperatures in particular, the interplay between quantum and thermal fluctuations may affect the nature of the condensation [39, 48, 72], thus giving rise to a richer phase diagram.

Notes Added. On finishing our manuscript, we became aware of a related preprint (arXiv:2209.10019), where the liquid-gas transition and the associated critical behavior are discussed in a different setup.

We thank Lan Yin and Shizhong Zhang for helpful discussions. This research is supported by NSFC under Grant Nos. 12174230 and 12147215 (Z.-Q.Y.), Grant No. 12104275 (L.H.), and Grant No. 11974331 (W.Y.); and partially by the Fund for Shanxi 1331 Project of Key Subjects Construction. W.Y. acknowledges support from the National Key R&D Program under Grant No. 2017YFA0304100.

-
- * These authors contributed equally to this work
† Electronic address: zqyu.physics@outlook.com
- [1] L. D. Landau and E. M. Lifshitz, *Statistical Physics*, Part 1 (Pergamon Press, New York, 1980).
 - [2] D. S. Petrov, Phys. Rev. Lett. **115**, 155302 (2015).
 - [3] H. Kadau, M. Schmitt, M. Wenzel, C. Wink, T. Maier, I. Ferrier-Barbut, and T. Pfau, Nature (London) **530**, 194 (2016).
 - [4] I. Ferrier-Barbut, H. Kadau, M. Schmitt, M. Wenzel, and T. Pfau, Phys. Rev. Lett. **116**, 215301 (2016).
 - [5] M. Schmitt, M. Wenzel, F. Böttcher, I. Ferrier-Barbut, and T. Pfau, Nature (London) **539**, 259 (2016).
 - [6] L. Chomaz, S. Baier, D. Petter, M. J. Mark, F. Wächtler, L. Santos, and F. Ferlaino, Phys. Rev. X **6**, 041039 (2016).
 - [7] F. Böttcher, M. Wenzel, J.-N. Schmidt, M. Guo, T. Langen, I. Ferrier-Barbut, T. Pfau, R. Bombín, J. Sánchez-Baena, J. Boronat, and F. Mazzanti, Phys. Rev. Research **1**, 033088 (2019).
 - [8] C. Cabrera, L. Tanzi, J. Sanz, B. Naylor, P. Thomas, P. Cheiney, and L. Tarruell, Science **359**, 301 (2018).
 - [9] G. Semeghini, G. Ferioli, L. Masi, C. Mazzinghi, L. Wolswijk, F. Minardi, M. Modugno, G. Modugno, M. Inguscio, and M. Fattori, Phys. Rev. Lett. **120**, 235301 (2018).
 - [10] P. Cheiney, C. R. Cabrera, J. Sanz, B. Naylor, L. Tanzi, and L. Tarruell, Phys. Rev. Lett. **120**, 135301 (2018).
 - [11] C. D’Errico, A. Burchianti, M. Prevedelli, L. Salasnich, F. Ancilotto, M. Modugno, F. Minardi, and C. Fort, Phys. Rev. Research **1**, 033155 (2019).
 - [12] Z. Guo, F. Jia, L. Li, Y. Ma, J. M. Hutson, X. Cui, and D. Wang, Phys. Rev. Research **3**, 033247 (2021).
 - [13] For reviews, see, F. Böttcher, J.-N. Schmidt, J. Hertkorn, K. S. H. Ng, S. D. Graham, M. Guo, T. Langen, and T. Pfau, Rep. Prog. Phys. **84**, 012403 (2021); Z.-H. Luo, W. Pang, B. Liu, Y.-Y. Li, and B. A. Malomed, Front. Phys. **16**, 32201 (2021).
 - [14] D. S. Petrov and G. E. Astrakharchik, Phys. Rev. Lett. **117**, 100401 (2016).
 - [15] F. Wächtler and L. Santos, Phys. Rev. A **93**, 061603(R) (2016).
 - [16] R. N. Bisset, R. M. Wilson, D. Baillie, and P. B. Blakie, Phys. Rev. A **94**, 033619 (2016).
 - [17] F. Wächtler and L. Santos, Phys. Rev. A **94**, 043618 (2016).
 - [18] M. Wenzel, F. Böttcher, T. Langen, I. Ferrier-Barbut, and T. Pfau, Phys. Rev. A **96**, 053630 (2017).
 - [19] A. Cappellaro, T. Macri, G. F. Bertacco, and L. Salasnich, Sci. Rep. **7**, 13358 (2017).
 - [20] D. Baillie and P. B. Blakie, Phys. Rev. Lett. **121**, 195301 (2018).
 - [21] C. Staudinger, F. Mazzanti, and R. E. Zillich, Phys. Rev. A **98**, 023633 (2018).
 - [22] V. Cikojević, K. Dželalija, P. Stipanović, L. Vranješ Markić, and J. Boronat, Phys. Rev. B **97**, 140502(R) (2018).
 - [23] F. Ancilotto, M. Barranco, M. Guilleumas, and M. Pi, Phys. Rev. A **98**, 053623 (2018).
 - [24] E. Chiquillo, Phys. Rev. A **97**, 063605 (2018).
 - [25] P. Zin, M. Pylak, T. Wasak, M. Gajda, and Z. Idziaszek, Phys. Rev. A **98**, 051603(R) (2018).
 - [26] T. Ilg, J. Kumlin, L. Santos, D. S. Petrov, and H. P.

- Büchler, Phys. Rev. A **98**, 051604(R) (2018).
- [27] N. B. Jørgensen, G. M. Bruun, and J. J. Arlt, Phys. Rev. Lett. **121**, 173403 (2018).
- [28] G. Ferioli, G. Semeghini, L. Masi, G. Giusti, G. Modugno, M. Inguscio, A. Gallemí, A. Recati, and M. Fattori, Phys. Rev. Lett. **122**, 090401 (2019).
- [29] V. Cikojević, L. V. Markić, G. E. Astrakharchik, and J. Boronat, Phys. Rev. A **99**, 023618 (2019).
- [30] L. Parisi, G. E. Astrakharchik, and S. Giorgini, Phys. Rev. Lett. **122**, 105302 (2019).
- [31] F. Minardi, F. Ancilotto, A. Burchianti, C. D’Errico, C. Fort, and M. Modugno, Phys. Rev. A **100**, 063636 (2019).
- [32] G. Ferioli, G. Semeghini, S. Terradas-Briansó, L. Masi, M. Fattori, and M. Modugno, Phys. Rev. Research **2**, 013269 (2020).
- [33] T. Mithun, A. Maluckov, K. Kasamatsu, B. A. Malomed, and A. Khare, Symmetry **12**, 174 (2020).
- [34] H. Hu and X.-J. Liu, Phys. Rev. Lett. **125**, 195302 (2020).
- [35] H. Hu, J. Wang, and X.-J. Liu, Phys. Rev. A **102**, 043301 (2020).
- [36] H. Hu and X.-J. Liu, Phys. Rev. A **102**, 053303 (2020).
- [37] Y. Wang, L. Guo, S. Yi, and T. Shi, Phys. Rev. Research **2**, 043074 (2020).
- [38] Q. Gu and L. Yin, Phys. Rev. B **102**, 220503(R) (2020).
- [39] L. He, P. Gao, and Z.-Q. Yu, Phys. Rev. Lett. **125**, 055301 (2020).
- [40] J. Wang, X.-J. Liu, and H. Hu, Chin. Phys. B **30**, 010306 (2021).
- [41] P. Zin, M. Pylak, and M. Gajda, Phys. Rev. A **103**, 013312 (2021).
- [42] L. Lavoine and T. Bourdel, Phys. Rev. A **103**, 033312 (2021).
- [43] R. N. Bisset, L. A. Peña Ardila, and L. Santos, Phys. Rev. Lett. **126**, 025301 (2021).
- [44] Joseph C. Smith, D. Baillie, and P. B. Blakie, Phys. Rev. Lett. **126**, 025302 (2021).
- [45] T. G. Skov, M. G. Skou, N. B. Jørgensen, and J. J. Arlt, Phys. Rev. Lett. **126**, 230404 (2021).
- [46] G. De Rosi, G. E. Astrakharchik, and P. Massignan, Phys. Rev. A **103**, 043316 (2021).
- [47] N. Guebli and A. Boudjemâa, Phys. Rev. A **104**, 023310 (2021).
- [48] H. Hu, Z.-Q. Yu, J. Wang, and X.-J. Liu, Phys. Rev. A **104**, 043301 (2021).
- [49] V. Cikojević, E. Poli, F. Ancilotto, L. Vranješ-Markić, and J. Boronat, Phys. Rev. A **104**, 033319 (2021).
- [50] M. N. Tengstrand and S. M. Reimann, Phys. Rev. A **105**, 033319 (2022).
- [51] Y. Xiong and L. Yin, Phys. Rev. A **105**, 053305 (2022).
- [52] T. A. Flynn, L. Parisi, T. P. Billam, and N. G. Parker, arXiv:2209.04318.
- [53] L. Tanzi, E. Lucioni, F. Famà, J. Catani, A. Fioretti, C. Gabbanini, R. N. Bisset, L. Santos, and G. Modugno, Phys. Rev. Lett. **122**, 130405 (2019).
- [54] F. Böttcher, J.-N. Schmidt, M. Wenzel, J. Hertkorn, M. Guo, T. Langen, and T. Pfau, Phys. Rev. X **9**, 011051 (2019).
- [55] L. Chomaz, D. Petter, P. Ilzhöfer, G. Natale, A. Trautmann, C. Politi, G. Durastante, R. M. W. van Bijnen, A. Patscheider, M. Sohmen, M. J. Mark, and F. Ferlaino, Phys. Rev. X **9**, 021012 (2019).
- [56] G. Natale, R. M. W. van Bijnen, A. Patscheider, D. Petter, M. J. Mark, L. Chomaz, and F. Ferlaino, Phys. Rev. Lett. **123**, 050402 (2019).
- [57] L. Tanzi, S. M. Rocuzzo, E. Lucioni, F. Famà, A. Fioretti, C. Gabbanini, G. Modugno, A. Recati and S. Stringari, Nature **574**, 382–385 (2019).
- [58] M. Guo, F. Böttcher, J. Hertkorn, J.-N. Schmidt, M. Wenzel, H. P. Büchler, T. Langen, and T. Pfau, Nature **574**, 386 (2019).
- [59] N. Navon, R. P. Smith and Z. Hadzibabic, Nat. Phys. **17**, 1334 (2021).
- [60] T. D. Lee, K. Huang, and C. N. Yang, Phys. Rev. **105**, 1119 (1957).
- [61] See Supplemental Material for details on the derivation of the phase boundaries, the hydrodynamic approach, and the critical phenomena, where Refs. [62–65] are included.
- [62] K. Huang, *Statistical Mechanics* (John Wiley & Sons, New York, 1987).
- [63] C. Pethick and H. Smith, *Bose-Einstein Condensation in Dilute Gases* (Cambridge University Press, New York, 2008).
- [64] J. Nespolo, G. E. Astrakharchik, and A. Recati, New J. Phys. **19**, 125005 (2017).
- [65] D. Romito, C. Lobo, and A. Recati, Phys. Rev. Research, **3**, 023196 (2021).
- [66] T. D. Lee, K. Huang, and C. N. Yang, Phys. Rev. **106**, 1135 (1957).
- [67] E. Feenberg, *Theory of Quantum Fluids* (Academic Press, New York, 1969).
- [68] L. P. Pitaevskii and S. Stringari, *Bose-Einstein Condensation and Superfluidity* (Oxford University Press, New York, 2016).
- [69] P. Naidon and D. S. Petrov, Phys. Rev. Lett. **126**, 115301 (2021).
- [70] A. Gammal, T. Frederico, L. Tomio, and Ph. Chomaz, Phys. Rev. A **61**, 051602(R) (2000).
- [71] A. Bulgac, Phys. Rev. Lett. **89**, 050402 (2002).
- [72] D. T. Son, M. Stephanov, and H. U. Yee, J. Stat. Mech. (2021) 013105.

Supplemental Material for

Quantum Criticality of Liquid-Gas Transition in a Binary Bose Mixture

Li He,¹ Haowei Li,² Wei Yi,^{2,3} and Zeng-Qiang Yu^{4,5}¹College of Physics and Electronic Engineering, Shanxi University, Taiyuan 030006, China²CAS Key Laboratory of Quantum Information, University of Science and Technology of China, Hefei 230026, China³CAS Center For Excellence in Quantum Information and Quantum Physics, Hefei 230026, China⁴Institute of Theoretical Physics, Shanxi University, Taiyuan 030006, China⁵State Key Laboratory of Quantum Optics and Quantum Optics Devices, Shanxi University, Taiyuan 030006, China

In this Supplementary Material, we provide details for the determination of the phase boundaries, the derivation of the response functions and density correlations, and the characterization of critical behaviors.

I. PHASE BOUNDARIES OF LIQUID-GAS COEXISTENCE

1.1 Approximate Solution of the Balance Conditions

In the PS-1 state defined in the main text, the system consists of a quantum-liquid component, coexisting with a gas of species 1. We determine the phase boundary of the PS-1 state from the balance conditions

$$\mu_1(n_1^L, n_2^L) = \mu_1(n_1^G, 0), \quad (\text{S1})$$

$$P(n_1^L, n_2^L) = P(n_1^G, 0), \quad (\text{S2})$$

where, as defined in the main text, n_1^L and n_2^L are the densities of different species in the liquid, and n_1^G is the density of the coexisting gas.

From Eq. (8) in the main text, one can reexpress the equilibrium densities using (n_+^L, n_-^L) and (n_+^G, n_-^G) . It follows from the equation of state (EOS) that, in the low-density regime with $n_i a^3 \lesssim \delta\tilde{g}^2$, we have $\left|\frac{\partial\mu_i}{\partial n_+}\right| \gg \left|\frac{\partial\mu_i}{\partial n_-}\right|$. Therefore, to meet the requirement of Eq. (S1), the hard-mode variable n_+ should differ little in the two coexisting phases. We then introduce $\Delta = n_+^L - n_+^G$. It can be checked that Δa^3 is a small quantity, at most of the order $\delta\tilde{g}^3$. Back in the (n_1, n_2) representation, we have

$$n_1^G = n_1^L - \lambda n_2^L - \Delta', \quad (\text{S3})$$

with Δ' being of the same order as Δ . Substituting Eq. (S3) into Eqs. (S1) and (S2), and keeping the relevant terms up to the order $\delta\tilde{g}^3$ and $\delta\tilde{g}^5$, respectively, we get

$$g_{11}\Delta' + \delta g n_2^L + \frac{4m^{3/2}}{3\pi^2\hbar^3} g_{11} \left[(g_{11}n_1^L + g_{22}n_2^L)^{3/2} - (g_{11}n_1^L - g n_2^L)^{3/2} \right] = 0, \quad (\text{S4})$$

$$(g_{11}n_1^L - g n_2^L) \Delta' + \delta g n_1^L n_2^L + \frac{4m^{3/2}}{5\pi^2\hbar^3} \left[(g_{11}n_1^L + g_{22}n_2^L)^{5/2} - (g_{11}n_1^L - g n_2^L)^{5/2} \right] = 0, \quad (\text{S5})$$

where $\delta g = g_{12} + g$. By eliminating Δ' , we obtain an analytical expression for the phase boundary

$$\lambda|\delta\tilde{g}|n_2^{L2} - \frac{32a^{3/2}}{15\sqrt{\pi}} \left[\left(\frac{n_1^L}{\lambda} + \lambda n_2^L \right)^{3/2} \left(5n_2^L + 3\lambda n_2^L - 2\frac{n_1^L}{\lambda} \right) + 2 \left(\frac{n_1^L}{\lambda} - n_2^L \right)^{5/2} \right] = 0. \quad (\text{S6})$$

It is then straightforward to recast Eq. (S6) into the dimensionless form given in the main text [Eq. (7) therein], by rescaling n_i^L with $n_i^{(0)}$.

We note that, at the specific density ratio $n_1/n_2 = \lambda$, Eq. (S6) reproduces the solution of self-bound state, $n_i^L = n_i^{(0)}$. When $n_2^L \rightarrow 0$, the phase boundary given by Eq. (S6) terminates at the critical point $(n_1^G, 0)$. The phase boundary of the PS-2 state can be obtained following a similar procedure, by switching the species labels. As illustrated in Fig. 1 of the main text, phase boundaries from the analytic expressions above agree well with those from numerical calculations.

1.2 Single-Mode Approximation

Since n_+ barely changes in the two coexisting phases, we can simplify calculations and gain further insight by taking the single-mode approximation, assuming

$$n_+^L = n_+^G. \quad (\text{S7})$$

Accordingly, we can determine the equilibrium structure from the single-variable EOS $\mathcal{E}(n_-)$, with a given n_+ . By applying the tangent Maxwell construction [1], the densities of the coexisting phases are fixed by

$$(n_-^L - n_-^G) \left. \frac{\partial \mathcal{E}}{\partial n_-} \right|_{n_-^L} = \mathcal{E}(n_-^L) - \mathcal{E}(n_-^G). \quad (\text{S8})$$

In the PS-1 state, the coexisting gas phase only consists of atoms of species 1, Eqs. (S7) and (S8) can then be rewritten as

$$n_1^G = n_1^L - \lambda n_2^L, \quad (\text{S9})$$

$$n_2^L [\lambda \mu_1(n_1^L, n_2^L) + \mu_2(n_1^L, n_2^L)] = \mathcal{E}(n_1^L, n_2^L) - \mathcal{E}(n_1^G, 0). \quad (\text{S10})$$

In deriving Eq. (S10), we have used $\left. \frac{\partial \mathcal{E}}{\partial n_-} \right|_{n_-^L} = \sin \theta \mu_1(n_1^L, n_2^L) + \cos \theta \mu_2(n_1^L, n_2^L)$.

Note that Eqs. (S9) and (S10) are not exactly equivalent to the balance conditions Eqs. (S1) and (S2). But the subtle difference between them does not affect the phase boundary, as long as the densities are kept to leading orders in $\delta \tilde{g}^2$. Explicitly, by using (S9) to eliminate n_1^G in (S10), one recovers Eq. (S6) for the phase boundary.

1.3 Case with Unequal Masses

In our calculations above, we assume the two species are of equal mass. For a heteronuclear mixture with unequal masses, one can still use n_+ and n_- to discern the hard and soft degrees of freedom for a virtual density variation. In the liquid-gas coexisting state, Eqs. (S9) and (S10) still hold within the single-mode approximation. Using the approximate EOS proposed in Ref. [2], we derive the phase boundary of the PS-1 state

$$\lambda |\delta \tilde{g}| n_2^{L2} - \frac{32a^{3/2}}{15\sqrt{\pi}} \left(\frac{\lambda}{\lambda'} \right)^{5/4} \left[\left(\frac{n_1^L}{\lambda} + \lambda' n_2^L \right)^{3/2} \left(5n_2^L + 3\lambda' n_2^L - 2\frac{n_1^L}{\lambda} \right) + 2 \left(\frac{n_1^L}{\lambda} - n_2^L \right)^{5/2} \right] = 0 \quad (\text{S11})$$

with $\lambda' = \left(\frac{m_2}{m_1} \right)^{3/5} \lambda$.

At the specific density ratio $n_1/n_2 = \lambda$, Eq. (S11) gives the self-bound solution $n_i^L = n_i^{(0)}$, with

$$n_i^{(0)} = \frac{25\pi}{1024 a^3} \sqrt{\frac{g}{g_{ii}}} \frac{\lambda'^{5/2}}{(1 + \lambda')^5} \delta \tilde{g}^2, \quad (\text{S12})$$

which is consistent with a previous result [3]. When $n_2^L \rightarrow 0$, the phase boundary terminates at the critical point $(n_1^C, 0)$, with

$$n_1^C = \frac{16}{25} (1 + \lambda') n_1^{(0)}. \quad (\text{S13})$$

Using the rescaled variables $\tilde{n}_i^L = n_i^L/n_i^{(0)}$, we can rewrite the phase boundary (S11) in a dimensionless form, which is the same as in the equal-mass case, except for the replacement of λ by λ' .

II. HYDRODYNAMIC APPROACH

In this section, we employ the hydrodynamic approach [4, 5] to study the density fluctuations in response to a weak, time-dependent perturbation, which are useful for identifying the critical phenomena. We consider the perturbative Hamiltonian

$$\hat{H}_{\text{pert}} = - \sum_{i=1,2} \alpha_i \hat{\rho}_{\mathbf{q},i}^\dagger e^{i\omega t + \eta t} + \text{H.c.}, \quad (\text{S14})$$

where $\hat{\rho}_{\mathbf{q},i}^\dagger$ is the density-fluctuation operator of species i with \mathbf{q} the wave vector, α_i is the perturbation strength, and ω is the frequency. The positive infinitesimal η ensures that the system is governed by the unperturbed Hamiltonian at $t = -\infty$. Below, we focus on the equal-mass case. The generalization to the unequal-mass case is straightforward.

2.1 Density Response Functions

Assuming the perturbation varies slowly in space, we write the energy of the system as a functional of the local density $n_i(\mathbf{r}, t)$

$$E = \int d\mathbf{r} \left[\sum_{i=1,2} \frac{\hbar^2}{2m} (\nabla \sqrt{n_i})^2 + \mathcal{E}(n_1, n_2) - \sum_{i=1,2} \alpha_i \left(n_i e^{i(\mathbf{q}\cdot\mathbf{r} - \omega t)} + \text{c.c.} \right) e^{\eta t} \right]. \quad (\text{S15})$$

Here we have omitted the kinetic energy term of the super flow, since it does not affect the density fluctuations in the linear response regime.

The evolution of the condensate wavefunction $\psi_i(\mathbf{r}, t) = \sqrt{n_i(\mathbf{r}, t)} e^{i\theta_i(\mathbf{r}, t)}$ is governed by the coupled equations

$$\frac{\partial n_i}{\partial t} + \frac{\hbar}{m} \nabla \cdot (n_i \nabla \theta_i) = 0, \quad (\text{S16})$$

$$\frac{\partial \theta_i}{\partial t} = -\frac{1}{\hbar} \frac{\delta E}{\delta n_i}, \quad (\text{S17})$$

where Eq. (S16) is the continuity equation, and Eq. (S17) is the generalization of the Josephson relation [4].

For small-amplitude density variance, Eq. (S16) and (S17) reduce to the linearized hydrodynamic equation

$$\frac{\partial^2}{\partial t^2} \delta n_i = -\frac{\hbar^2}{4m^2} \nabla^2 (\nabla^2 \delta n_i) + \frac{n_i}{m} \sum_{j=1,2} \frac{\partial \mu_i}{\partial n_j} \delta n_j + \alpha_i n_i \frac{q^2}{m} \left(e^{i(\mathbf{q}\cdot\mathbf{r} - \omega t)} + \text{c.c.} \right) e^{\eta t}, \quad (\text{S18})$$

whose solution can be written as

$$\delta n_i(\mathbf{r}, t) = \sum_{j=1,2} \alpha_j \left[\chi_{ij}(q, \omega) e^{i(\mathbf{q}\cdot\mathbf{r} - \omega t)} + \text{c.c.} \right] e^{\eta t}. \quad (\text{S19})$$

Here $\chi_{ij}(q, \omega)$ is the species-resolved density response function

$$\chi_{ii}(q, \omega) = \frac{2\epsilon_q n_i}{m(c_+^2 - c_-^2)} \sum_{\ell=\pm} \ell \frac{\gamma_{3-i} n_{3-i} - m c_\ell^2}{\hbar^2 [(\omega + i\eta)^2 - \omega_{q,\ell}^2]}, \quad (\text{S20})$$

$$\chi_{12}(q, \omega) = \chi_{21}(q, \omega) = -\frac{2\epsilon_q \gamma_{12} n_1 n_2}{m(c_+^2 - c_-^2)} \sum_{\ell=\pm} \frac{\ell}{\hbar^2 [(\omega + i\eta)^2 - \omega_{q,\ell}^2]}, \quad (\text{S21})$$

with $\epsilon_q = \hbar^2 q^2 / 2m$, and the energy of elementary excitations $\hbar\omega_{q,\ell} = \sqrt{\epsilon_q(\epsilon_q + 2m c_\ell^2)}$. The expressions for the sound velocities c_\pm are given in the following subsection.

2.2 Sound Velocity

The long-wavelength excitations consist of two phonon modes: the lower-branch ($\ell = -$) corresponds to the in-phase density oscillation, and the upper-branch ($\ell = +$) corresponds to the out-of-phase oscillation. The sound velocities of the two branches are given by

$$c_\pm = \sqrt{\frac{1}{2m} \left[\gamma_1 n_1 + \gamma_2 n_2 \pm \sqrt{(\gamma_1 n_1 - \gamma_2 n_2)^2 + 4\gamma_{12}^2 n_1 n_2} \right]}, \quad (\text{S22})$$

which are positive when the species densities exceed the threshold marked by the diffusive spinodal. For the self-bound liquid ($n_i = n_i^{(0)}$), we find

$$c_+^{(0)} = \sqrt{\frac{gn^{(0)}}{m}} \left[1 + \frac{8}{\sqrt{\pi}} \left(\lambda + \frac{1}{\lambda} - \frac{4}{5} \right) \sqrt{n^{(0)}a^3} \right], \quad (\text{S23})$$

$$c_-^{(0)} = 4\sqrt{\frac{gn^{(0)}}{5\sqrt{\pi}m}} \sqrt{n^{(0)}a^3}. \quad (\text{S24})$$

Our expression for $c_-^{(0)}$ above is consistent with previous results based on the Beliaev theory [6, 7] to leading orders in $|\delta\tilde{g}|^{3/2}$.

We note that, in our hydrodynamic theory, the Andreev-Bashkin effect is not taken into account, which would result in a minor correction to the sound velocity [8, 9]. In general, such a correction mainly affects the out-of-phase phonon mode, and its magnitude is much smaller than that of the Lee-Huang-Yang term [9].

2.3 Structure Factor and Correlation Lengths

According to the fluctuation-dissipation theorem, $S_{ij}(q) = \frac{\hbar}{\pi\sqrt{n_i n_j}} \int_0^\infty d\omega \text{Im}\chi_{ij}(q, \omega)$, we construct the static structure factor

$$S_{ii}(q) = \frac{\epsilon_q}{m(c_+^2 - c_-^2)} \sum_{\ell=\pm} \ell \frac{mc_\ell^2 - \gamma_{3-i}n_{3-i}}{\hbar\omega_{q,\ell}}, \quad (\text{S25})$$

$$S_{12}(q) = S_{21}(q) = \frac{\epsilon_q}{m(c_+^2 - c_-^2)} \sum_{\ell=\pm} \ell \frac{\gamma_{12}\sqrt{n_1 n_2}}{\hbar\omega_{q,\ell}}. \quad (\text{S26})$$

The structure factor $S_{ij}(q)$ is further related to the pair-distribution function $\mathcal{D}_{ij}(r)$ through the relation [5, 10]

$$\mathcal{D}_{ij}(r) = 1 + \frac{1}{\sqrt{n_i n_j}} \int \frac{d\mathbf{q}}{(2\pi)^3} [S_{ij}(q) - \delta_{ij}] e^{-i\mathbf{q}\cdot\mathbf{r}}. \quad (\text{S27})$$

In the long-wavelength limit, $S_{ij}(q)$ is a linear function of q , which can be explicitly written as

$$S_{ij}(q \rightarrow 0) = \frac{q\xi_{ij}}{\sqrt{2}}. \quad (\text{S28})$$

Accordingly, at large distance, the asymptotic form of \mathcal{D}_{ij} reads [10]

$$\mathcal{D}_{ij}(r \rightarrow \infty) = 1 - \frac{\xi_{ij}}{\sqrt{2n_i n_j} \pi^2 r^4}. \quad (\text{S29})$$

Equation (S28) can be viewed as a definition of the correlation lengths ξ_{ij} . Therein, the prefactor $\frac{1}{\sqrt{2}}$ is introduced to be consistent with the usual convention in a single-component Bose gas. From Eq. (S25) and (S26), we obtain

$$\xi_{ii} = \frac{\hbar}{\sqrt{2}m(c_+ + c_-)} \left(1 + \frac{\gamma_{3-i}n_{3-i}}{mc_+c_-} \right) \quad (\text{S30})$$

$$\xi_{12} = \xi_{21} = -\frac{\hbar}{\sqrt{2}} \frac{\gamma_{12}\sqrt{n_1 n_2}}{m^2(c_+ + c_-)c_+c_-}. \quad (\text{S31})$$

III. CRITICAL BEHAVIOR OF LIQUID-GAS TRANSITION

In this section, we present details in characterizing the critical behaviors, including divergent susceptibility, phonon-mode softening, and enhanced correlation lengths. These quantities are derived using the hydrodynamic approach presented in the previous section.

3.1 Divergent Susceptibility

The susceptibility is defined by the static density response in the long-wavelength limit, $\chi_{ij}^0 \equiv \chi_{ij}(q \rightarrow 0, \omega = 0)$ [5]. From Eqs. (S20) and (S21), we derive

$$\chi_{ii}^0 = \frac{\gamma_{3-i}}{\gamma_1 \gamma_2 - \gamma_{12}^2}, \quad (\text{S32})$$

$$\chi_{12}^0 = \chi_{21}^0 = \frac{-\gamma_{12}}{\gamma_1 \gamma_2 - \gamma_{12}^2}, \quad (\text{S33})$$

which are consistent with the thermodynamic relation $\chi_{ij}^0 = \left(\frac{\partial n_i}{\partial \mu_j} \right)_{\mu_{3-j}}$. Apparently, all the static susceptibilities diverge at the critical points, where the phase boundary of the liquid-gas coexistence meets the spinodal line (see Fig. 1 of the main text).

3.2 Phonon-Mode Softening

At either critical point, the sound velocity vanishes along with the minority density. But it is the linear density dependence of the sound velocity that stands out as a critical phenomenon. Specifically, for n_1 fixed at n_1^c , a straightforward small- n_2 expansion of c_- gives

$$c_- = n_2 \sqrt{\frac{1}{m} \frac{\partial}{\partial n_2} \left(\gamma_2 - \frac{\gamma_{12}^2}{\gamma_1} \right)} \Big|_{(n_1, n_2) = (n_1^c, 0)} = \frac{5\sqrt{\lambda}}{2\sqrt{2}} c_-^{(0)} \tilde{n}_2, \quad (\text{S34})$$

where in the second equality we have used Eq. (S24). Such a linear dependence only occurs at the critical point. Indeed, for any fixed $n_1 > n_1^c$, the expansion yields

$$c_- = 2\sqrt{1 + \lambda} c_-^{(0)} \sqrt{\tilde{n}_2 \left(\sqrt{\frac{n_1}{n_1^c}} - 1 \right)}. \quad (\text{S35})$$

The clear distinction between Eq. (S34) and (S35) is illustrated in Fig. 3(a) of the main text.

3.3 Enhanced Correlation Lengths.

From Eqs. (S30) and (S31), it is also straightforward to derive the critical correlation lengths. For n_1 fixed at n_1^c , the correlation lengths in the small minority-density limit behave like

$$\xi_{11} \xrightarrow{n_2 \rightarrow 0} \xi_1^{\text{single}} \left(1 + \frac{1}{\sqrt{|\delta \tilde{g}|}} \right), \quad (\text{S36})$$

$$\xi_{12} \xrightarrow{n_2 \rightarrow 0} \frac{\xi^{(0)}}{\sqrt{3(1 + \lambda)} \tilde{n}_2} \rightarrow \infty, \quad (\text{S37})$$

$$\xi_{22} \xrightarrow{n_2 \rightarrow 0} \frac{4 \xi^{(0)}}{5\sqrt{3\lambda} \tilde{n}_2} \rightarrow \infty. \quad (\text{S38})$$

By contrast, for any fixed $n_1 > n_1^c$, we have in the small minority-density limit

$$\xi_{11} \xrightarrow{n_2 \rightarrow 0} \xi_1^{\text{single}}, \quad (\text{S39})$$

$$\xi_{12} \xrightarrow{n_2 \rightarrow 0} \frac{5\sqrt{\lambda}}{4\sqrt{6}(1 + \lambda)} \frac{\xi^{(0)}}{\sqrt{\frac{n_1}{n_1^c} \left(\sqrt{\frac{n_1}{n_1^c}} - 1 \right)}}, \quad (\text{S40})$$

$$\xi_{22} \xrightarrow{n_2 \rightarrow 0} \frac{\xi_0}{\sqrt{6(1 + \lambda) \left(\sqrt{\frac{n_1}{n_1^c}} - 1 \right)} \tilde{n}_2} \rightarrow \infty \quad (\text{S41})$$

These are illustrated in Fig. 3(b)(c)(d) of the main text.

-
- [1] K. Huang, *Statistical Mechanics* (John Wiley & Sons, New York, 1987).
 - [2] F. Minardi, F. Ancilotto, A. Burchianti, C. D'Errico, C. Fort, and M. Modugno, *Phys. Rev. A* **100**, 063636 (2019).
 - [3] V. Cikojević, E. Poli, F. Ancilotto, L. Vranješ-Markić, and J. Boronat, *Phys. Rev. A* **104**, 033319 (2021).
 - [4] C. Pethick and H. Smith, *Bose-Einstein Condensation in Dilute Gases* (Cambridge University Press, New York, 2008).
 - [5] L. P. Pitaevskii and S. Stringari, *Bose-Einstein Condensation and Superfluidity* (Oxford University Press, New York, 2016).
 - [6] Q. Gu and L. Yin, *Phys. Rev. B* **102**, 220503(R) (2020).
 - [7] Y. Xiong and L. Yin, *Phys. Rev. A* **105**, 053305 (2022).
 - [8] J. Nespolo, G. E. Astrakharchik, and A. Recati, *New J. Phys.* **19**, 125005 (2017).
 - [9] D. Romito, C. Lobo, and A. Recati, *Phys. Rev. Research*, **3**, 023196 (2021).
 - [10] E. Feenberg, *Theory of Quantum Fluids* (Academic Press, New York, 1969).